Defect modes in photonic crystal slabs studied using terahertz time-domain spectroscopy

Zhongping Jian, Jeremy Pearce, and Daniel M. Mittleman

Department of Electrical and Computer Engineering, Rice University, MS-366, P.O. Box 1892, Houston, Texas 77251-1892

Received March 31, 2004

We describe broadband coherent transmission studies of two-dimensional photonic crystals consisting of a hexagonal array of air holes in a dielectric slab in a planar waveguide. By filling several of the air holes in the photonic crystal slab, we observe the signature of a defect mode within the stop band, in both the amplitude and phase spectra. The experimental results are in reasonable agreement with theoretical calculations using the transfer matrix method. © 2004 Optical Society of America

OCIS codes: 320.7100, 230.7400, 260.3090.

Recent years have seen increasing interest in the use of terahertz (THz) radiation for a variety of applications.[1] This trend has led to an increasing need for quasi-optical components that can be used to manipulate THz beams. One promising candidate is photonic crystals. Early research on photonic bandgap materials used THz radiation to probe millimeter- and submillimeter-scale structures as a means for understanding the properties of periodic media in a regime where the fabrication was less challenging than at optical frequencies.[2–8] More recently, the motivation has shifted toward the optimization of structures specifically intended for use at THz frequencies.[9–16] These experiments have primarily focused on defect-free photonic crystals. Only a few studies of the properties of THz defect modes have been reported.[4,9,17,18] However, it is clear that, just as at optical frequencies, the utility of THz photonic crystals relies on the incorporation of defect structures to disrupt the periodicity and thereby introduce propagating modes within the bandgap.[19]

Here we report measurements of a two-dimensional (2D) photonic crystal slab in which functional structures (such as resonant cavities or waveguides) can be incorporated and removed, reversibly. As with several previous authors, we employ THz time-domain spectroscopy for transmission measurements.[7,8,11,13] This technique provides a direct measurement of the THz electric field, which is generated in the form of a single-cycle pulse. As a result, both the amplitude and the phase of the radiation can be determined experimentally.

As a first demonstration, we study a 2D planar waveguide with a periodic dielectric modulation in the plane. Specifically, we have used deep reactive-ion etching to pattern a high-resistivity silicon wafer with a hexagonal array of circular holes.[14] The holes have diameters of 360 μm, with a pitch of 400 μm. The calculated 2D band structure for this photonic crystal is shown in Fig. 1.[20]

This slab geometry mimics the most commonly employed configuration used in near-infrared applications, in which light is confined in two dimensions by the photonic crystal and in the third by waveguiding.[19] In our samples the 300-μm thickness of the slab is large enough to support not only the fundamental TEM mode but also one set of higher modes (the E_{10} and H_{10} modes[21]) at the highest frequency of interest (the top of the bandgap, near 0.4 THz). We have chosen to operate in this multimode regime to optimize the coupling efficiency of radiation from free space into the slab waveguide. We note that undistorted single-mode propagation can still be achieved, even at frequencies above the cutoff of higher-order modes, if the incident beam is mode matched to the (dispersionless) TEM mode.[22] In the situation described here the higher modes are of odd parity[21] and therefore are not efficiently excited by the incident wave.

The experimental setup (Fig. 1) is similar to previous THz waveguide measurements.[23] Broadband single-cycle THz pulses are generated and detected

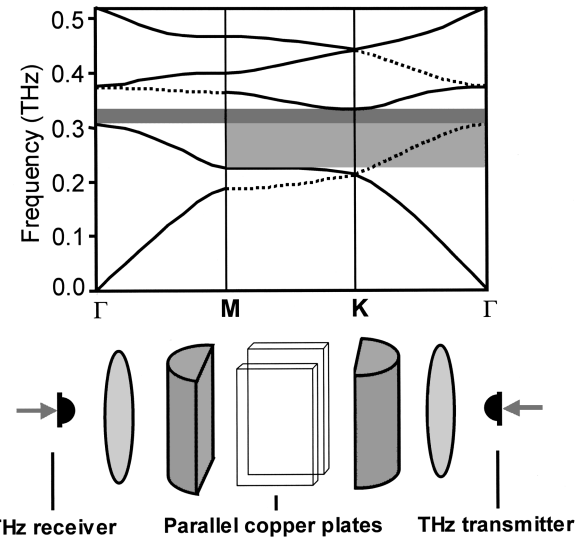

Fig. 1. Top, 2D band structure (TM polarization) of the photonic crystal used in these measurements. This band structure is computed assuming an infinite slab thickness.[20] The shaded boxes indicate the full gap (darker) and the pseudogap (lighter), and the dashed bands are antisymmetric and therefore do not couple to the incident beam. Bottom, schematic of the experimental setup. The photonic crystal is placed within the copper waveguide for transmission measurements.

0146-9592/04/172067-03$15.00/0

with photoconducting antennas.[1] The THz radiation is focused into a parallel-plate copper waveguide by a plano–cylindrical lens. The incident field is polarized perpendicular to the plane of the waveguide (TM polarized). An identical setup is used at the exit facet to collect the transmitted radiation. The photonic crystal slab is sandwiched inside the metal waveguide, which provides a nearly ideal lossless boundary for the guided wave.[23] We have etched the wafer over only half of its area, leaving an unetched portion that we use to collect a reference transmission spectrum.

Figure 2 shows several typical measured waveforms, probing the $\Gamma-K$ direction of the 2D hexagonal lattice. When there is no silicon wafer inside the waveguide, we observe the expected distortionless propagation, as reported previously for broadband pulses.[23,24] When the unetched silicon wafer is inserted into the waveguide, the cutoff wavelength for each waveguide mode shrinks by a factor of the refractive index, $n = 3.42$.[21] As a result, a larger fraction of the input pulse energy (which extends to beyond 1 THz) overlaps the dispersive modes, so we observe some pulse dispersion as well as an overall delay of the signal. However, when the etched portion of the wafer (the photonic crystal) is illuminated, the waveform is substantially dispersed, extending to hundreds of picoseconds. This dramatic dispersion results from sharp spectral features in the photonic band structure such as the edges of the stop band.[25–28] We observe that the earliest peak of the signal arrives roughly 19 ps earlier than the corresponding peak in the case of the solid silicon waveguide (bottom inset of Fig. 2). Given the propagation distance (four unit cells along $\Gamma-K$), we compute a mean dielectric of 3.9 for the photonic crystal, which is close to the volume-weighted average value of 3.86.

We introduce a defect structure into the otherwise perfect photonic crystal by filling several of the air holes with a finely ground powder of high-resistivity silicon. The grain size of this powder ($\sim$10 μm) is much smaller than the shortest wavelength used in our measurement, so it acts as a homogeneous medium with a dielectric somewhat smaller than that of bulk crystalline silicon. Figure 3(a) shows the transmission spectrum of the photonic crystal, referenced to that of the unetched silicon slab, in the vicinity of the photonic bandgap. The addition of the three-point defect gives rise to an enhanced transmission in the middle of the gap, near 0.28 THz. On removal of the defect, this resonance vanishes.

Figure 3(b) shows a calculated transmission spectrum for these two experimental situations (with and without defect), obtained using the transfer-matrix method (TMM).[29,30] We note that these simulations assume a 2D lattice with infinite extent in the third dimension. So we do not expect perfect correspondence with the experimental results. However, we note that the metal cladding in our structures eliminates the light cone states, extending perpendicular to the slab.[31] As a result one might expect these 2D simulations to be more accurate than in the case of dielectric-clad slabs. We also note that the dielectric constant of the composite material filling the three holes is not known with any precision. We use a representative value of $\epsilon = 5.0$ for these illustrative calculations.

The TMM spectra contain many features similar to those observed in the data. We observe a systematic shift between the experimental and the computed locations of the band edges of $\sim$0.025 THz. This shift was

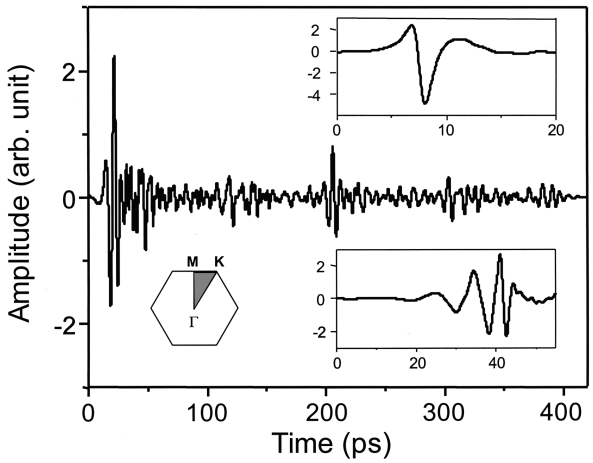

Fig. 2. Typical time-domain THz waveform measured in transmission through the photonic crystal slab. Insets, waveform when the waveguide contains air (top) and a solid silicon slab (bottom). In all three cases the distance between the two copper plates is 300 μm, the thickness of the photonic crystal slab.

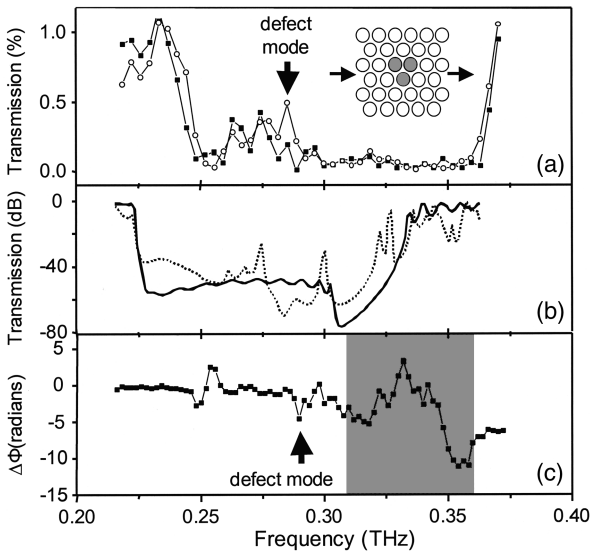

Fig. 3. (a) Experimental transmission spectrum for the photonic crystal, relative to a solid silicon slab of equal thickness. Filled squares, perfect lattice; open circles, the same lattice but with three holes filled in the pattern shown in the inset. A defect mode appears at $\sim$0.28 THz. (b) Solid curve, TMM calculation for a perfect photonic crystal; dotted curve, lattice with a three-point defect. The material filling the holes is assumed to be a uniform dielectric with $\epsilon = 5.0$. (c) Difference in the spectral phases of the two measured waveforms that gave the spectra in (a). The signature of the defect mode is evident at 0.28 THz. The shaded area denotes the region of the full photonic bandgap, where the transmitted intensity is not large enough for accurate determination of the phase.

previously attributed to the finite thickness of the photonic crystal slab,[14,31,32] an effect that is not accounted for in the TMM simulation. The calculation also predicts narrow enhanced transmission peaks similar to the one observed in the data. Several defect modes, near the upper and lower edges of the complete gap, are not observed in the experiment. Finally, we note that the high-frequency portion of the stop band corresponds to the full 2D gap for TM polarization, whereas the lower portion corresponds only to a pseudogap, in which the bands support antisymmetric mode patterns that do not couple strongly to the incident radiation.[2,17] As a result the transmission coefficient is somewhat higher in this low-frequency region, a result echoed in our experimental findings.

We take advantage of this somewhat larger transmission to obtain the dispersion associated with the defect mode. The time-domain spectroscopy technique provides a direct measure of the spectral phase of the THz wave. Ordinarily, obtaining this spectrum would be quite challenging for radiation inside the stop band, since the transmitted intensity is so small. However, the combination of the slightly higher transmission (resulting from the fact that the defect mode lies in a pseudogap rather than inside the complete gap) with the excellent dynamic range of the measurement permits us to extract phase information across the defect mode. Figure 3(c) shows the phase difference ($\phi_{\text{defect}} - \phi_{\text{no defect}}$) obtained from the measured waveforms. Because the defect mode introduces both amplitude and phase changes for propagation near the resonance frequency, we expect to see a signature of the defect at ~0.28 THz in this difference spectrum. This feature is indicated by an arrow in Fig. 3(c).

In conclusion, we have studied transmission properties of a two-dimensional photonic crystal slab with metal cladding, using terahertz time-domain spectroscopy. By filling several holes with a fine powder, defect modes are reversibly introduced to the photonic crystal lattice. These modes can be characterized in both amplitude and phase. The amplitude transmission spectra are in reasonable agreement with TMM calculations. These results highlight the power of time-domain spectroscopy for characterizing photonic lattices.

The authors acknowledge useful conversations with Rajesh Rengarajan and Tushar Prasad. This work was supported in part by the National Science Foundation. D. M. Mittleman's e-mail address is daniel@rice.edu.

References

1. D. M. Mittleman, *Sensing with Terahertz Radiation* (Springer-Verlag, Berlin, 2003).
2. W. M. Robertson, G. Arjavalingam, R. D. Meade, K. D. Brommer, A. M. Rappe, and J. D. Joannopoulos, Phys. Rev. Lett. **68,** 2023 (1992).
3. E. Ozbay, E. Michel, G. Tuttle, R. Biswas, K. M. Ho, J. Bostak, and D. M. Bloom, Opt. Lett. **19,** 1155 (1994).
4. E. Ozbay, J. Opt. Soc. Am. B **13,** 1945 (1996).
5. M. C. Wanke, O. Lehmann, K. Müller, Q. Wen, and M. Stuke, Science **275,** 1284 (1997).
6. G. Feiertag, W. Ehrfeld, H. Freimuth, H. Kolle, H. Lehr, M. Schmidt, M. M. Sigalis, C. M. Soukoulis, G. Kiriakidis, T. Pedersen, J. Kuhl, and W. Koenig, Appl. Phys. Lett. **71,** 1441 (1997).
7. A. Chelnokov, S. Rowson, J.-M. Lourtioz, L. Duvillaret, and J.-L. Coutaz, Electron. Lett. **33,** 1981 (1997).
8. T. Aoki, M. W. Takeda, J. W. Haus, Z. Yuan, M. Tani, K. Sakai, N. Kawai, and K. Inoue, Phys. Rev. B **64,** 045106 (2001).
9. F. Gadot, A. de Lustrac, J.-M. Lourtioz, T. Brillat, A. Ammouche, and E. Akmansoy, J. Appl. Phys. **85,** 8499 (1999).
10. C. Jin, B. Cheng, Z. Li, D. Zhang, L.-M. Li, and Z.-Q. Zhang, Opt. Commun. **166,** 9 (1999).
11. H. Kitahara, N. Tsumura, H. Kondo, M. W. Takeda, J. W. Haus, Z. Yuan, N. Kawai, K. Sakoda, and K. Inoue, Phys. Rev. B **64,** 045202 (2001).
12. R. Gonzalo, I. Ederra, C. M. Mann, and P. de Maagt, Electron. Lett. **37,** 613 (2001).
13. H. Han, H. Park, M. Cho, and J. Kim, Appl. Phys. Lett. **80,** 2634 (2002).
14. N. Jukam and M. S. Sherwin, Appl. Phys. Lett. **83,** 21 (2003).
15. S.-W. Wang, W. Lu, X.-S. Chen, Z.-F. Li, X.-C. Shen, and W. Wen, J. Appl. Phys. **93,** 9401 (2003).
16. T. D. Drysdale, R. J. Blaikie, and D. R. S. Cumming, Appl. Phys. Lett. **83,** 5362 (2003).
17. M. Wada, K. Sakoda, and K. Inoue, Phys. Rev. B **52,** 16297 (1995).
18. B. Temelkuran, M. Bayindir, E. Ozbay, J. P. Kavanaugh, M. M. Sigalas, and G. Tuttle, Appl. Phys. Lett. **78,** 264 (2001).
19. J. D. Joannopoulos, R. D. Meade, and J. N. Winn, *Photonic Crystals: Molding the Flow of Light* (Princeton U. Press, Princeton, N.J., 1995).
20. S. Johnson and J. D. Joannopoulos, "MIT photonic-bands," http://ab-initio.mit.edu/mpb (1999).
21. N. Marcuvitz, *Waveguide Handbook* (McGraw-Hill, New York, 1951).
22. G. Gallot, S. P. Jamison, R. W. McGowan, and D. R. Grischkowsky, J. Opt. Soc. Am. B **17,** 851 (2000).
23. R. Mendis and D. Grischkowsky, Opt. Lett. **26,** 846 (2001).
24. R. Mendis and D. Grischkowsky, IEEE Microwave Wireless Components Lett. **11,** 444 (2001).
25. A. Imhof, W. L. Vos, R. Sprik, and A. Lagendijk, Phys. Rev. Lett. **83,** 2942 (1999).
26. Y. A. Vlasov, S. Petit, G. Klein, B. Honerlage, and C. Hirlimann, Phys. Rev. E **60,** 1030 (1999).
27. M. C. Netti, C. E. Finlayson, J. J. Baumberg, M. D. B. Charlton, M. E. Zoorob, J. S. Wilkinson, and G. J. Parker, Appl. Phys. Lett. **81,** 3927 (2002).
28. T. Asano, K. Kiyota, D. Kumamoto, B.-S. Song, and S. Noda, Appl. Phys. Lett. **84,** 4690 (2004).
29. J. B. Pendry and A. MacKinnon, Phys. Rev. Lett. **69,** 2772 (1992).
30. TMM software supplied by A. L. Reynolds, University of Glasgow, Scotland, UK.
31. S. G. Johnson, S. Fan, P. R. Villeneuve, J. D. Joannopoulos, and L. A. Kolodziejski, Phys. Rev. B **60,** 5751 (1999).
32. D. M. Whittaker, J. S. Culshaw, V. N. Astratov, and M. S. Skolnick, Phys. Rev. B **65,** 073102 (2002).